

The SLUGGS Survey: New evidence for a tidal interaction between the early type galaxies NGC 4365 and NGC 4342

Christina Blom,^{1*} Duncan A. Forbes,¹ Caroline Foster,^{2,3}

Aaron J. Romanowsky^{4,5} and Jean P. Brodie⁵

¹*Centre for Astrophysics and Supercomputing, Swinburne University, Hawthorn, VIC 3122, Australia*

²*Australian Astronomical Observatory, PO Box 915, North Ryde, NSW 1670, Australia*

³*European Southern Observatory, Alonso de Cordova 3107, Vitacura, Santiago 19001, Chile*

⁴*Department of Physics and Astronomy, San José State University, 1 Washington Square, San Jose, CA 95192, USA*

⁵*University of California Observatories, 1156 High St., Santa Cruz, CA 95064, USA*

* Email: cblom@astro.swin.edu.au

15 November 2021

ABSTRACT

We present new imaging and spectral data for globular clusters (GCs) around NGC 4365 and NGC 4342. NGC 4342 is a compact, X-ray luminous S0 galaxy with an unusually massive central black hole. NGC 4365 is another atypical galaxy that dominates the W' group of which NGC 4342 is a member. Using imaging from the MegaCam instrument on the Canada-France-Hawaii Telescope (CFHT) we identify a stream of GCs between the two galaxies and extending beyond NGC 4342. The stream of GCs is spatially coincident with a stream/plume of stars previously identified. We find that the photometric colours of the stream GCs match those associated with NGC 4342, and that the recession velocity of the combined GCs from the stream and NGC 4342 match the recession velocity for NGC 4342 itself. These results suggest that NGC 4342 is being stripped of GCs (and stars) as it undergoes a tidal interaction with the nearby elliptical galaxy NGC 4365. We compare NGC 4342 to two well-known, tidally stripped galaxies (M32 and NGC 4486B) and find various similarities. We also discuss previous claims by Bogdán et al. (2012a) that NGC 4342 cannot be undergoing significant tidal stripping because it hosts a large dark matter halo.

Key words: galaxies: elliptical and lenticular, cD - galaxies: evolution - galaxies: formation - galaxies: individual: NGC 4365, NGC 4342 - galaxies: kinematics and dynamics - galaxies: star clusters: general

1 INTRODUCTION

Λ CDM cosmology predicts that the giant galaxies we see in the local Universe have been built up to their present size by successive mergers of galaxies and accretion of small galaxies. Globular clusters (GCs) are very useful tracers of these merger and accretion events as they are dense and mostly robust to the violent interactions of galaxies. Additionally, several extragalactic spectroscopic studies have found that the overwhelming majority of GCs are > 10 Gyrs old (Strader et al. 2005). Therefore, most of the GCs that we observe locally were formed very early in the evolution of the Universe and have survived all the interactions their host galaxies were involved in. They have likely undergone several galaxy merger events, or have been stripped off smaller galaxies, and accumulated around large galaxies over time

(Côté et al. 1998; Tonini 2013). They should maintain a chemical signature of the conditions they were formed under and a kinematic signature of the processes by which they were acquired by large galaxies (West et al. 2004).

NGC 4365 is a giant elliptical galaxy with a redshift independent distance measurement of 23.1 Mpc (Blakeslee et al. 2009) and a recession velocity of 1243 km s⁻¹ (Smith et al. 2000), placing it ~ 6 Mpc behind the Virgo Cluster. NGC 4365 is the central galaxy in the W' group and has been noted to have rare properties for a galaxy of its luminosity. It has a kinematically distinct core and the bulk of its stars rotate along the minor axis (Surma & Bender 1995; Davies et al. 2001; Krajnović et al. 2011, Arnold et al. 2013 in prep.), while its GC system consists of three sub-populations (Puzia et al. 2002; Larsen et al. 2005; Brodie et al. 2005; Blom et al. 2012a,b) rather than the usual two

(Brodie & Strader 2006; Peng et al. 2006). It has recently been studied as part of the SAGES Legacy Unifying Globulars and GalaxyS (SLUGGS¹; Brodie et al. in preparation) Survey.

NGC 4342 is a small S0 galaxy 20 arcmin away from NGC 4365 with a recession velocity of 751 km s^{-1} (Grogin et al. 1998) but its distance has not been measured independently of redshift. Recently, Jiang et al. (2012) searched the Seven Samurai Survey (Faber et al. 1989) and highlighted it as a local example of a high redshift superdense ‘red nugget’ (Daddi et al. 2005; van Dokkum et al. 2008) and it has long been known to have an oversized central supermassive black hole for its bulge mass (Cretton & van den Bosch 1999).

In the last year, Bogdán et al. (2012a) presented a very deep B filter image of NGC 4365 showing a stellar stream extending from NE of NGC 4365, across the elliptical galaxy, bridging the gap between NGC 4365 and NGC 4342, and extending further SW. This image has prompted investigation of the nature of the interaction between NGC 4365 and NGC 4342. Bogdán et al. (2012b) found X-ray emitting hot gas around NGC 4342. This presents an interesting puzzle regarding the origin of the stellar stream. It appears as if the stellar material has been tidally stripped off NGC 4342 as it passed by NGC 4365 and what remains of NGC 4342 is now swinging back towards NGC 4365. However, the presence of X-ray emitting gas around NGC 4342 suggests a large dark matter halo that should not be present if stars have been stripped off the galaxy.

Here we investigate the interaction between NGC 4365 and NGC 4342 using GCs, assessing what the spatial, colour and velocity distributions of the GCs around NGC 4342 and NGC 4365 indicate about the nature of the interaction between these two galaxies. In particular, is NGC 4365 stripping stars and GCs off NGC 4342 or is there another explanation?

We describe the photometric selection of GC candidates and detail our analysis of the properties of the spatial and colour distributions of the GC system in Section 2. Section 3 contains the reduction and analysis of the spectroscopic data, the kinematic selection of GCs as well as a kinematic analysis of the stream and NGC 4342 GCs. In Section 4 we investigate the effects of tidal stripping with respect to galaxy scaling relations and present a counter-argument to some of the findings of Bogdán et al. (2012a), before discussing the results and concluding the paper in Sections 5 and 6 respectively.

2 PHOTOMETRIC ANALYSIS

2.1 Imaging Data

We use the public archival data from the MegaCam instrument on the Canada-France-Hawaii Telescope (CFHT) to identify GC candidates in the area around NGC 4342 and NGC 4365. The square degree u filter image stack is centred on R.A. = 185.912° and Decl. = 7.0562° (J2000.0) with a total exposure time of 4240 s. The g and i filter image stacks are centred on R.A. = 186.133° and Decl. = 7.2708° (J2000.0), and have total exposure times of 3170 and 2055

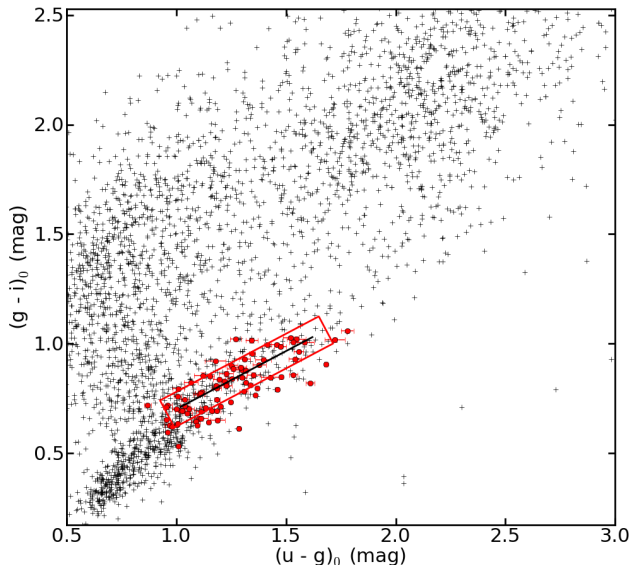


Figure 1. Colour selection of globular cluster (GC) candidates. $(g - i)_0$ colour is plotted against $(u - g)_0$ colour. The black crosses show all point sources brighter than $i = 21$ mag and red dots show the objects matched with NGC 4365 GC candidates selected from Subaru/Suprime-Cam photometry (Blom et al. 2012a). The previously photometrically selected GC candidates form a linear correlation, shown with a black line. We select additional GC candidates that are consistent, within individual errors (not shown), with the red $\pm 2\sigma$ box around the line.

s respectively. The overlap of the three image stacks covers an area of ~ 0.66 square degrees, encompassing NGC 4365, NGC 4342 and almost all of the stellar stream (Bogdán et al. 2012a). We use catalogues produced by the MegaPipe data reduction pipeline (Gwyn 2008), operated by the Canadian Astronomy Data Centre (CADC), to spatially match point sources found in all three image stacks. The faintest i magnitude of included objects is 23.0 mag. We correct for foreground reddening, using $A_u = 0.11$, $A_g = 0.08$ and $A_i = 0.04$, determined from Galactic dust maps (Schlegel et al. 1998).

2.2 Globular cluster candidate selection

The selection of GC candidates from the matched point sources is shown in Figure 1. The figure shows $(g - i)_0$ colour plotted against $(u - g)_0$ colour for the point sources in the field-of-view, as well as the NGC 4365 GC candidates used to identify the locus of GCs in colour-colour space. These NGC 4365 GC candidates were matched in spatial coordinates between the MegaPipe catalogues and previous work using the Subaru/Suprime-Cam (S-Cam) instrument, with a 35×27 arcmin² field-of-view (Blom et al. 2012a). We use the S-Cam identified GC candidates to fit a line to the GC distribution, then expand the line by $\pm 2\sigma$ to form a box and select candidates that overlap that box within individual errors. The spectroscopically confirmed GCs from Blom et al. (2012b) are consistent with this box. Given the $i = 23.0$ mag cutoff, the mean individual errors in the GC candidate sample are ± 0.1 mag in $(u - g)_0$ colour and ± 0.04 mag in $(g - i)_0$ colour. We identify a total of 1786 GC candidates that meet these criteria.

¹ <http://sluggs.swin.edu.au>

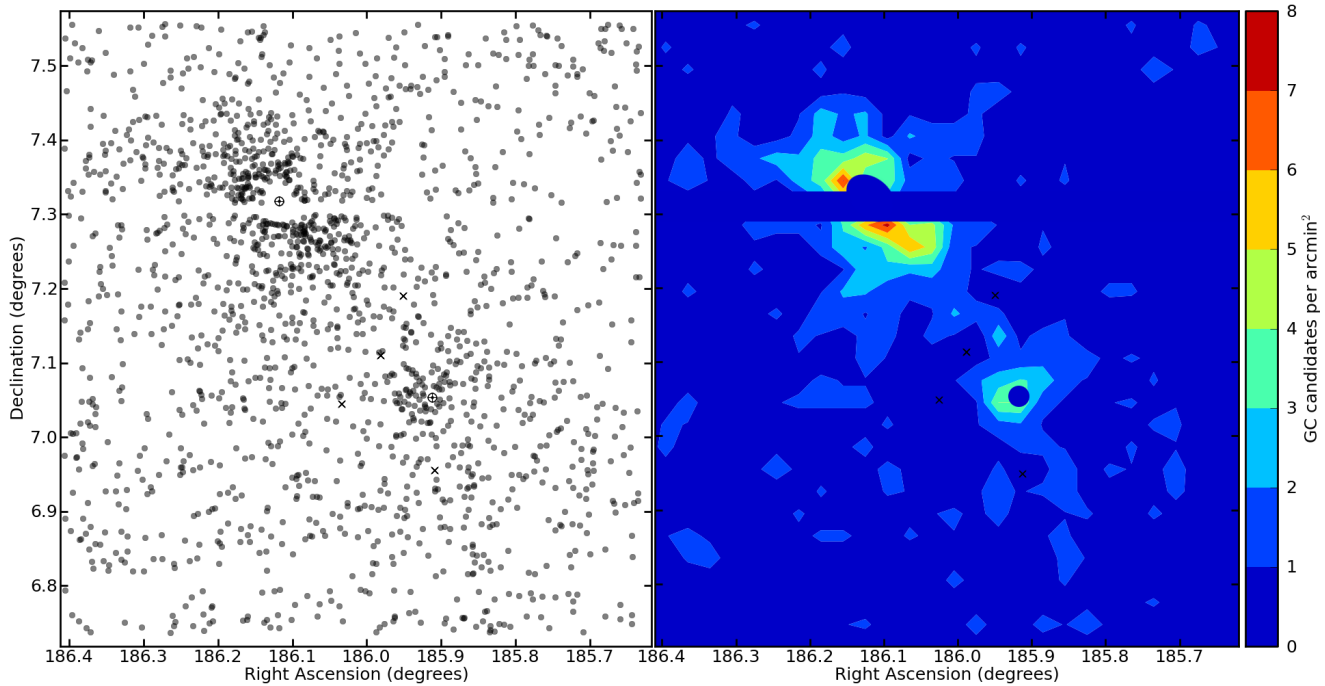


Figure 2. Spatial distribution of globular cluster (GC) candidates around NGC 4342 and NGC 4365. **(Left)** Individual GC candidates are shown as grey dots and the two galaxies are shown with circles circumscribing crosses (NGC 4365 towards the top left and NGC 4342 towards the bottom right). The two-dimensional distribution of the GC candidates shows a clear overdensity around NGC 4365 and NGC 4342. There are several galaxies in the region that are as bright as NGC 4342 (marked with X's) but none show a similar GC overdensity. The horizontal void running through the centre of NGC 4365 is due to a CCD chip problem in the u filter. GC candidates are not recovered in the very central regions of NGC 4365 and NGC 4342 due to the high galaxy surface brightness there. **(Right)** The two-dimensional spatial distribution of GC candidates smoothed to a resolution of 1.8 arcmin. Here we see an overdensity of GC candidates not only around NGC 4342 and NGC 4365 but also between the two galaxies and South West of NGC 4342 that is spatially coincident with the stellar stream. The spatial coincidence of the elongated GC candidate overdensity and the recently reported stellar stream (Bogdán et al. 2012a) is highly unlikely to be a chance occurrence. Both galaxy centres and the horizontal void are blocked in the smoothed image.

2.3 Spatial distribution

Given the selection of GC candidates, Figure 2 shows their spatial distribution. The first panel shows the unsmoothed 2D surface density map. We see a GC overdensity corresponding to NGC 4365's GC system and we find an overdensity of GC candidates around NGC 4342. The absolute magnitude of NGC 4342 ($M_B = -18.45$ mag for a distance of 23.1 Mpc) is comparable to that of several other galaxies superimposed on the stellar stream (i.e. NGC 4341: $M_B = -17.68$, NGC 4343: $M_B = -19.46$, IC 3267: $M_B = -17.7$, IC 3259: $M_B = -17.91$, assuming the same distance as NGC 4342); however we do not see a clear overdensity associated with any of them. None of the superimposed galaxies are likely to be significantly more distant than NGC 4342 (see their quoted recession velocities in Figure 11). We find that NGC 4342 has an order of magnitude more GC candidates than the nearby galaxies of similar luminosity, indicating that it is significantly underluminous for its GC system.

The 2D distribution of GC candidates is smoothed to a spatial resolution of 1.8 arcmin in the second panel of Figure 2. Once the data are smoothed the GC candidate overdensity along the stellar stream is also apparent. The GC overdensity bridges the gap between NGC 4365 and NGC 4342 and extends further SW of NGC 4342, in roughly the same

line as the bridge part of the GC stream. This result is robust to small variations in the magnitude cut and the spatial resolution of the smoothing. The number of GC candidates contributing to the visible stream overdensities is on the order of tens of objects and it is conceivable that such a stream structure could arise by chance. This possibility is testable if the distribution of GCs expected from both NGC 4365 and NGC 4342 was simulated and compared with the actual spatial distribution. In order to simulate the spatial distribution of the GC contribution from these two galaxies, their radial and azimuthal distributions need to be determined.

2.3.1 Spatial properties of the GC system of NGC 4342

With ~ 140 photometrically observed GC candidates in the spatial overdensity seen around NGC 4342 in the left panel of Figure 2 we can determine some of the quantitative parameters of the GC distribution. The radial surface density of GC candidates, shown in Figure 3, is calculated in annuli around NGC 4342. No GC candidates are detected within 0.5 arcmin from the centre of NGC 4342 because the high starlight surface brightness there inhibits object detection. Consequently the first radial bin (between 0.5 and 1.5 arcmin) is possibly also affected by this incompleteness. (We are unable to quantify this possible incompleteness because the original images on which object detection was based are

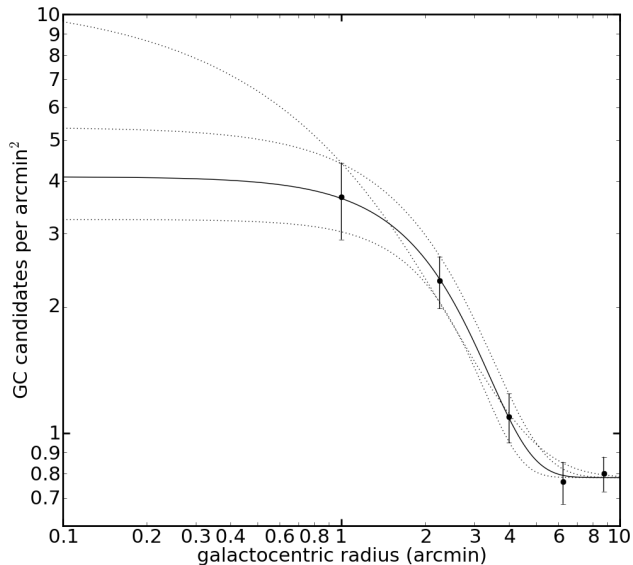


Figure 3. Radial surface density of GC candidates brighter than $i = 23$ mag around NGC 4342 plotted against galactocentric radius. The dots with error bars show the surface density points, and the best fit Sérsic profile (with an additional background term) is plotted with a solid line. The ranges of Sérsic parameters that would still fit the data points within errors are also shown. The two dotted lines forming an envelope to the best fit line show the minimum and maximum range for the fitted parameters (P_e , R_e , n) respectively. The third dotted line shows a Sérsic profile where the shape parameter n is 2.3 times the best fit value, consistent with all the data points. The data are well matched by the Sérsic profile fit but without data points closer than 1 arcmin from the galaxy centre it is not possible to constrain the fit well. See text for further details.

not publicly available.) To ensure that there are significant GC candidate numbers in each bin we divide the data into only five annuli and fit a Sérsic profile added to a background term to these. The Sérsic profile with background term (bg) is given by (Graham & Driver 2005):

$$P(R) = P_e \exp \left(-b_n \left[\left(\frac{R}{R_e} \right)^{\frac{1}{n}} - 1 \right] \right) + bg \quad (1)$$

where

$$b_n = 1.9992n - 0.3271, \quad (2)$$

P_e is the density at the effective radius, R_e is the effective radius of the GC system, and n is the shape parameter of the Sérsic profile. The best fit profile is given by:

$$\begin{aligned} P_e &= 1.68 \pm 0.19 \text{ arcmin}^{-2} \\ R_e &= 2.12 \pm 0.12 \text{ arcmin} \\ n &= 0.50 \pm 0.12 \\ bg &= 0.782 \pm 0.025 \text{ arcmin}^{-2} \end{aligned}$$

The values of the background term and the effective radius of the GC system are well constrained by the five surface density values obtainable from the MegaCam data set. Here the value for the background surface density will include non-GC contamination and GCs that are spatially associated with the stellar stream rather than NGC 4342 itself. We measure the effective radius of NGC 4342's GC

system to be 2.12 ± 0.12 arcmin (~ 14 kpc) compared with the stellar effective radius of 0.5 arcmin (~ 3 kpc) (de Vaucouleurs et al. 1991). The best fit profile is plotted on Figure 3. The truncation of NGC 4342 GCs at ~ 5 arcmin is secure and we can conclude that the bound GC system of NGC 4342 does not extend beyond ~ 34 kpc. It is unusual for a GC system to have a value < 1 for the shape parameter n (Rhode & Zepf 2004; Spitler et al. 2006, 2008; Pota et al. 2013) and we also plot a Sérsic profile where $n = 1.15$, as we suspect that the fitted error for n is underestimated due to the small dataset. The data cannot rule out this ($n = 1.15$) fit as it is consistent within errors with every data point. To improve the constraint on the shape parameter n , more GC data are needed in the central regions of the galaxy. To probe further into the centre of NGC 4342 better imaging and careful subtraction of the galaxy light is required. If n is indeed < 1 , the GC system of NGC 4342 is sharply truncated, which could be an argument for tidal stripping.

We measure the angle of each GC candidate bound to NGC 4342 (within 5 arcmin) with respect to the centre of the galaxy. Angles start at 0° directly North of the galaxy centre and progress anti-clockwise to 180° directly South of the centre. To increase the signal-to-noise we fold the data at 180° and plot the binned data in Figure 4. This fold preserves any sinusoidal signature of ellipticity. The azimuthal distribution of the GC candidates still bound to NGC 4342 is consistent with being circular. Even with azimuthal bins encompassing 18 degrees in radius, the distribution of GC candidates does not show a significant peak at any one position angle. It is possible that deeper imaging, probing fainter GCs and closer to the galaxy centre would show a small but significant ellipticity in the bound GCs. The photometric major axis position angle of NGC 4342 is 166° and it would be interesting to determine if the GC distribution position angle is consistent with that of the galaxy or the stellar stream ($\sim 45^\circ$).

2.3.2 Statistical significance of the GC overdensity on the stream

We generated 1000 simulated GC spatial distributions around NGC 4365 and NGC 4342 of which Figure 5 is an example. These distributions are the addition of a uniform background sampling added to a sampling from the spatial distributions of both NGC 4365 and NGC 4342. Each simulated spatial distribution contains 2000 objects. This number was conservatively chosen to be higher than the number of objects in the observed distribution (1786) because there are voids in the observed spatial distribution. The background was set at a density of 0.5 arcmin^{-2} across the entire area. This value was chosen to visually match the object density far from NGC 4365, NGC 4342 and the stream on the CFHT/MegaCam observations. The background value of 0.78 measured in Section 2.3.1 is likely to include stream GCs as well as non-GC contaminating objects. The rejection method was used to extract random positions according to the spatial distribution functions. We used the Sérsic profile and azimuthal distribution fitted by Blom et al. (2012a) to simulate the radial and azimuthal distribution of NGC 4365 and the previously fitted Sérsic profile for NGC 4342. The Sérsic profile was noted to be highly uncertain in the inner regions of NGC 4342, but the fitted profile is sufficient for

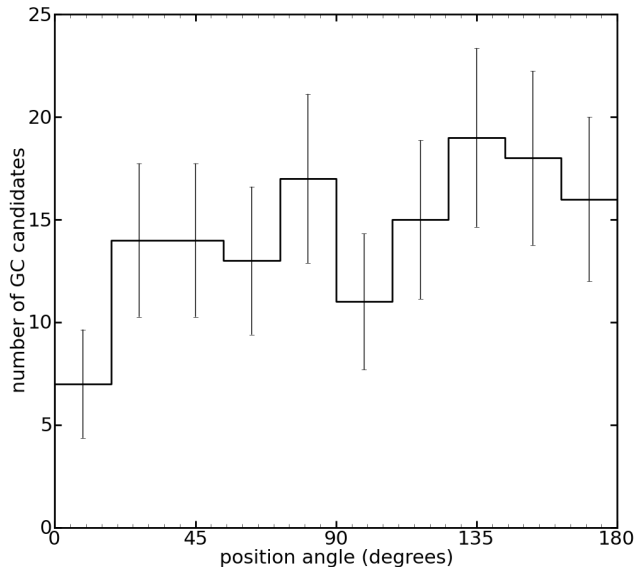


Figure 4. Azimuthal distribution of GC candidates within 5 arcmin from the centre of NGC 4342 and brighter than $i = 23$ mag. The position angle of 0° is directly North of NGC 4342’s centre and increases anti-clockwise. The data are folded at 180° , preserving any elliptical signature while increasing signal-to-noise. This distribution indicates that the GC system of NGC 4342 is consistent with zero ellipticity (a circular GC distribution). If the GC distribution was significantly elliptical the azimuthal distribution would show a clear sinusoidal shape with the peak of the distribution at the position angle of the elliptical distribution. The photometric position angle of NGC 4342 is 166° .

these purposes as we are primarily concerned with the outer regions of both galaxies’ spatial distributions. No significant differences are seen in the outer regions of simulated spatial distributions when the value of the Sérsic profile n parameter is greater than 1. Figure 5 also shows the specific areas which were compared to the observed spatial distribution.

The overdensity in the two stream areas was calculated by dividing the density in the stream defined areas by the density in the off-stream areas alongside (see Figure 5) and then added together. For the observed spatial distribution we calculated a summed stream overdensity of 3.53. We also calculated the overdensity of the region NW of NGC 4365 and found the overdensity there to be 2.94. The observed overdensities are compared with the distribution of overdensities in Figure 6. A summed overdensity equal to or greater than the observed value on the stream between NGC 4365 and NGC 4342 as well as on the stream beyond NGC 4342 occurs by chance only 2.2 percent of the time (2.3σ in a normal distribution). An overdensity in the regions NW of NGC 4365 occurs by chance only 0.1 percent (3.3σ) of the time. The overdensity NW of NGC 4365 is spatially coincident with the background galaxy NGC 4334 ($V = 4354$ km s $^{-1}$) and it is likely that the GC candidate overdensity there is associated with that galaxy, although spectroscopic observations would be required to test that further.

The GC candidate distribution along the stream is highly unlikely to occur by chance and is best explained by tidal stripping of GCs from one galaxy by another.

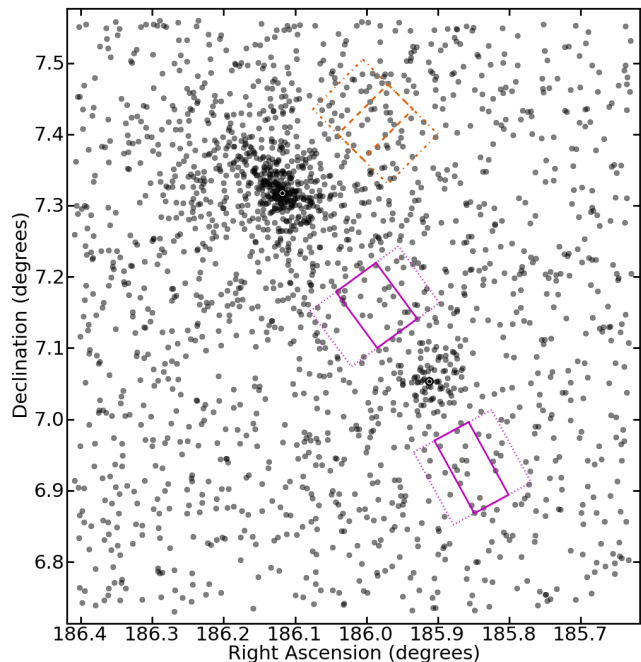


Figure 5. An example of the 1000 simulations of the spatial distribution of the GCs around NGC 4365 and NGC 4342. Each simulated spatial distribution contains 2000 GC candidates, created by the addition of a uniform background, the Sérsic profile of NGC 4342 GCs and the spatial distribution of NGC 4365 GCs. NGC 4365’s GC spatial distribution includes the Sérsic profile and azimuthal distribution fitted in Blom et al. (2012a). The solid magenta regions mark the areas of stream overdensity between the two galaxies and SW of NGC 4342. These stream overdensities can be seen in Figure 2. The dotted magenta off-stream regions on either side of the solid boxes are used to compare off-stream densities. The dashed orange region marks the position of an overdensity to the NW of NGC 4365 also visible in Figure 2 and the dash-dotted region marks the comparison area.

2.4 Colour distribution

We have calculated the transformation from $(g' - i')_0$ in the SDSS photometric system (used for the S-Cam photometry) to $(g - i)_0$ in the MegaCam photometric system. The data used for the calculation and the resulting transformation are shown in Figure 7. We find a shift of -0.102 mag from the SDSS to MegaCam colours that is not strongly dependent on $(g - i)_0$ colour over the colour range of GC candidates.

Comparing the colour distributions of GC candidates associated with NGC 4365, NGC 4342 and the stellar stream (see Figure 8) we see a significant population of red (metal-rich) GC candidates present in NGC 4365’s GC system that is absent from the colour distribution of either the stream or NGC 4342. We do not probe the central regions of NGC 4342 where red GCs are likely to be found and if the GCs are tidally stripped from the outskirts of NGC 4342 we also do not expect metal rich GCs in the stream. There is no significant difference between the GC colour distribution of the stream population and that of NGC 4342, whereas the blue colour of both stream and NGC 4342 GC candidates are not a good match for the colour of the blue GC candidates of NGC 4365. This supports the theory that the stream GCs are actually GCs from the outer parts of NGC 4342’s GC

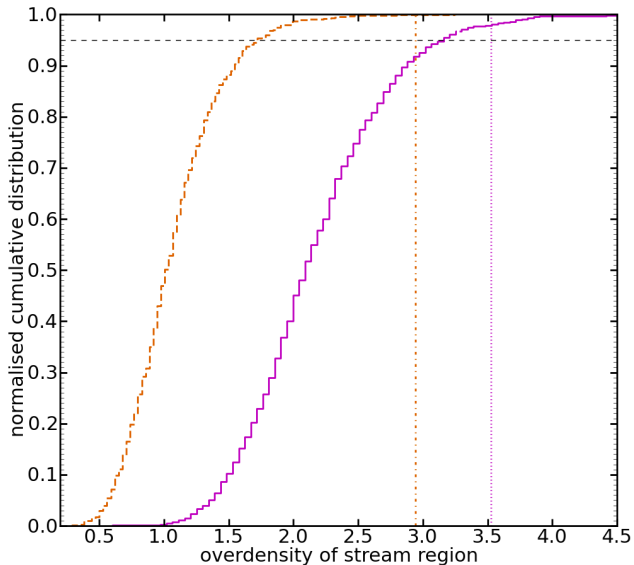


Figure 6. Cumulative distribution of the calculated stream overdensity for 1000 simulated GC spatial distributions. The solid magenta line shows the on-stream density divided by the off-stream density for the stream region between the two galaxies and SW of NGC 4342 added together. The dashed orange line shows the same overdensity parameter for the region NW of NGC 4365. The dash-dotted orange and dotted magenta lines show the overdensity measured in the same regions for the observed GC candidate spatial distribution. The horizontal black dashed line shows the 95th percentile. The intersection of the vertical measured overdensity lines and cumulative distribution lines fall well above the 95th percentile. The overdensity NW of NGC 4365 is possibly associated with the background galaxy NGC 4334.

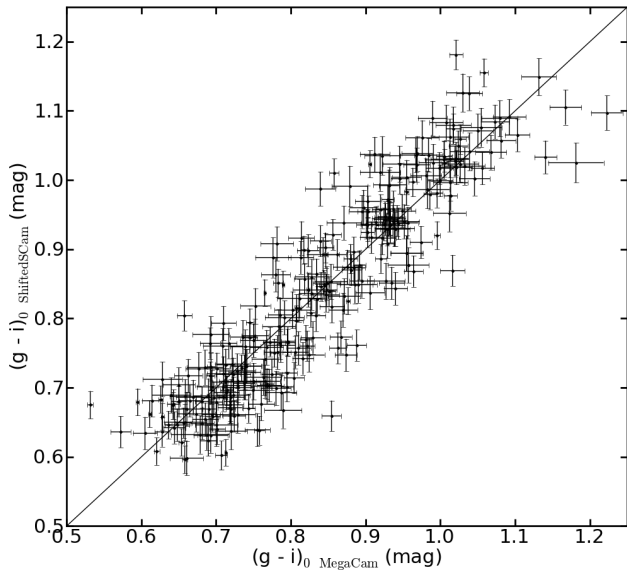


Figure 7. Scaling between Subaru/Suprime-Cam ($g' - i'$)₀ and CFHT/MegaCam ($g - i$)₀ colours. Points with error bars are the objects with photometry from both S-Cam and MegaCam and MegaCam i magnitude brighter than 23 mag. The black line shows a one-to-one correlation between the ($g - i$)₀ colours. The S-Cam colours have been shifted by -0.102 mag and the comparison between shifted S-Cam and MegaCam colours is consistent with a one-to-one correlation over the GC colour range.

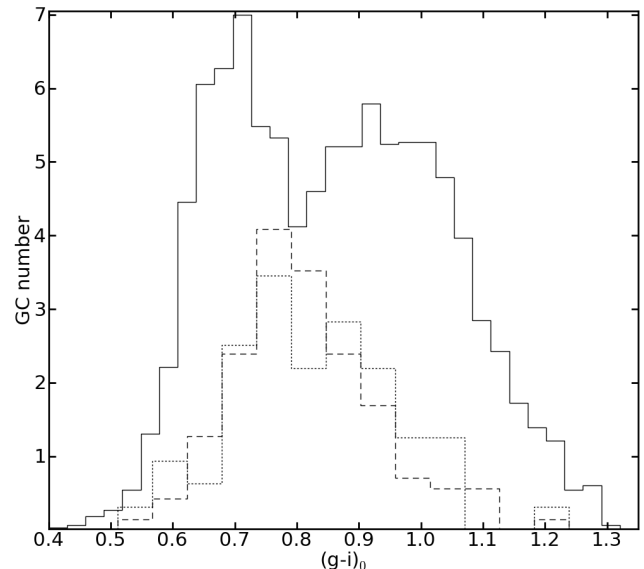


Figure 8. Histogram of ($g - i$)₀ GC colours for NGC 4365, NGC 4342 and the stellar stream. The colour distribution of GC candidates within 5 arcmin of NGC 4342 is plotted with a dashed line and the colour distribution of candidates that overlap with the stream regions as defined in Figures 2 and 5 is plotted with a dotted line. The colour distribution of NGC 4365 is scaled to 33 percent of its height and plotted with a solid line. It has been shifted from Subaru/Suprime-Cam ($g' - i'$)₀ (Blom et al. 2012a) to CFHT/MegaCam ($g - i$)₀ colours and scaled down for comparison. The colour distribution of NGC 4342's GC system is indistinguishable from the colour distribution of the GC stream and both lack the red GCs seen in the colour distribution of NGC 4365's GC system.

system that have been stripped off the galaxy during a tidal interaction with NGC 4365.

3 SPECTROSCOPIC ANALYSIS

3.1 Spectroscopic Data

Three slitmasks were observed on 2012, April 17 with the DEep Imaging Multi-Object Spectrograph (DEIMOS) on the Keck II telescope (Faber et al. 2003). The slitmasks were positioned along the stream South West of NGC 4365 and around NGC 4342. GC candidates within each slitmask were prioritized for observation based on their brightness. The slitmasks were each observed for a total of 2 hours, split over 4 observations of 30 min each. The median seeing was 1.2 arcseconds. For all 3 masks, the slits were 1 arcsecond wide and a 1200 l/mm grating, centred on 7800 Å, was used in conjunction with the OG550 filter. This setup (Pota et al. 2013) enables observations from $\sim 6550 - 8900$ Å with a wavelength resolution of ~ 1.5 Å. The Calcium II triplet (CaT) absorption features (8498, 8542 and 8662 Å) are within the observed wavelength range up to recession velocities of ~ 8200 km s⁻¹. This includes NGC 4342 ($V = 751$ km s⁻¹, Grogin, Geller & Huchra 1998) and NGC 4365 ($V = 1243$ km s⁻¹ Smith et al. 2000). We use these absorption features to determine the line-of-sight velocity for each candidate GC.

The data were reduced using a modified version of the

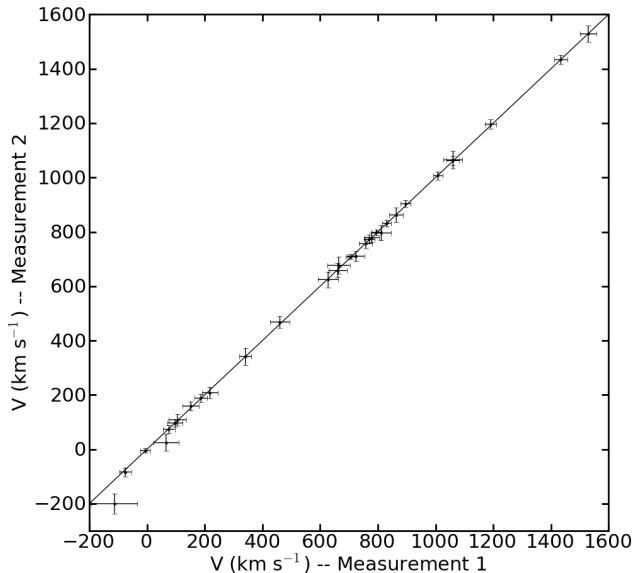


Figure 9. Comparison of independent velocity measurements from DEIMOS spectra. Velocities are plotted with error bars on a one-to-one relationship line. All the velocities are consistent with each other except the lowest velocity. We exclude this object from further analysis and measure an rms dispersion about the one-to-one line of 8.8 km s^{-1} .

DEEP2 (Deep Extragalactic Evolutionary Probe 2) galaxy survey data reduction pipeline (IDL SPEC2D Cooper et al. 2012; Newman et al. 2012). The pipeline uses dome flats, NeArKrXe arc lamp spectra and sky light visible in each slit to perform flat fielding, wavelength calibration and local sky subtraction, respectively. The object spectrum was cross correlated (using the IRAF task RV.FXCOR) with the CaT features in 13 stellar template spectra observed with the same setup. The velocity of the object is calculated by taking the mean of the 13 cross correlation values and the uncertainty on the velocity is calculated by adding in quadrature the standard deviation of the velocities and the mean of the errors on those velocities (as determined by RV.FXCOR). The process of velocity determination was independently repeated by a second investigator and results are shown in Figure 9. We only include a velocity measurement in further analysis, if it has a reliable velocity (as determined by both investigators) and the measured velocities are consistent within the measured uncertainties (i.e. the 1σ error bar of one measurement overlaps the other velocity measurement). The root-mean-squared dispersion between the two independent measurements is 8.8 km s^{-1} .

3.2 Velocity selection

If the GC candidates on the stream and around NGC 4342 originate from the same system, we expect their recession velocities to be similar. A superposition of NGC 4342 GCs on a population of stream GCs that have been stripped from another, now completely disrupted galaxy, might show a large offset in recession velocity.

We find 33 objects with measurable recession velocities between -200 and 1600 km s^{-1} but assume the 11 objects with velocities smaller than 400 km s^{-1} to be stars in our own Galaxy. The remaining 21 GCs are plotted in Figure 10

I.D.	R.A.	Decl.	V	V _{err}	(g - i) ₀
	(degrees)		(km s ⁻¹)		(mag)
1	185.9401	7.031459	1060.96	32.67	0.739
2	185.9213	7.035125	863.96	24.33	0.666
3	185.9598	7.045965	706.69	16.77	0.846
4	185.9558	7.045967	831.14	14.73	0.708
5	185.9771	7.048600	758.41	22.65	0.911
6	185.9753	7.082502	795.31	17.96	0.861
7	185.9512	7.099172	897.06	17.68	0.786
8	186.0573	7.182025	627.83	35.51	0.854
9	185.7894	6.944254	870.57	20.42	0.674
10	185.8825	6.988903	811.86	34.09	0.953
11	185.8480	7.014668	769.10	41.91	0.741
12	185.9185	7.019106	770.51	19.25	0.773
13	185.8866	7.040393	661.51	32.29	0.727
14	185.9483	7.063918	778.85	25.04	0.814
15	185.7881	7.030769	724.31	29.35	0.696
16	185.8933	7.083244	1008.32	16.11	0.748
17	185.8355	7.081957	460.64	33.42	0.775
18	185.8873	7.147331	664.27	39.24	0.758
19	186.0902	7.243450	796.64	11.37	0.925
20	186.1140	7.328690	538.85	7.39	0.984
21	186.0164	7.152190	519.93	9.97	0.870
22	186.0573	7.182080	624.60	6.26	0.659
23	186.0640	7.224360	734.53	5.15	0.760
24	186.1108	7.315610	698.58	15.57	0.923
25	186.1011	7.325980	712.22	12.39	0.845
26	186.1203	7.300140	720.09	8.61	0.712
27	186.1341	7.368620	682.49	14.93	1.077
28	186.0563	7.251730	758.64	12.42	0.642
29	186.1403	7.175740	668.30	4.22	0.808
30	186.1637	7.145680	797.62	5.46	0.680
31	186.0988	7.293170	673.24	4.55	0.877

Table 1. Positions, recession velocities and photometric colours (CFHT/MegaCam) for the 31 GCs associated with NGC 4342 and the stream. GCs numbered 1 to 18 are presented for the first time in this work and GCs numbered 19 to 31 are low velocity outliers previously presented in Blom et al. (2012b).

showing GC recession velocity against galactocentric radius from NGC 4365. We no longer refer to these as GC candidates because their recession velocity has been confirmed. The new velocities presented in this work scatter about the recession velocity of NGC 4342 ($V = 751 \text{ km s}^{-1}$). The velocities of GCs around NGC 4365 are also shown along with the 2σ dispersion envelopes as a function of galactocentric radius. As highlighted in Blom et al. (2012b), there is a grouping of low velocity GCs that are also consistent with NGC 4342's recession velocity.

Four of the 22 GCs with measured velocities are more likely to be associated with NGC 4365 than NGC 4342 and the stream. Two have significantly higher velocities than NGC 4342 ($> 1400 \text{ km s}^{-1}$) and another two have reasonably high velocities ($> 1050 \text{ km s}^{-1}$); all are radially consistent with NGC 4365's GC system. We associate 18 new GC recession velocities with the sample of 13 stream GCs identified in Blom et al. (2012b) giving a total of 31 GCs associated with NGC 4342 and the stream. The positions, recession velocities and photometric colours of these GCs are listed in Table 1. We conclude that GCs associated with NGC 4342 and the stream are indistinguishable in velocity.

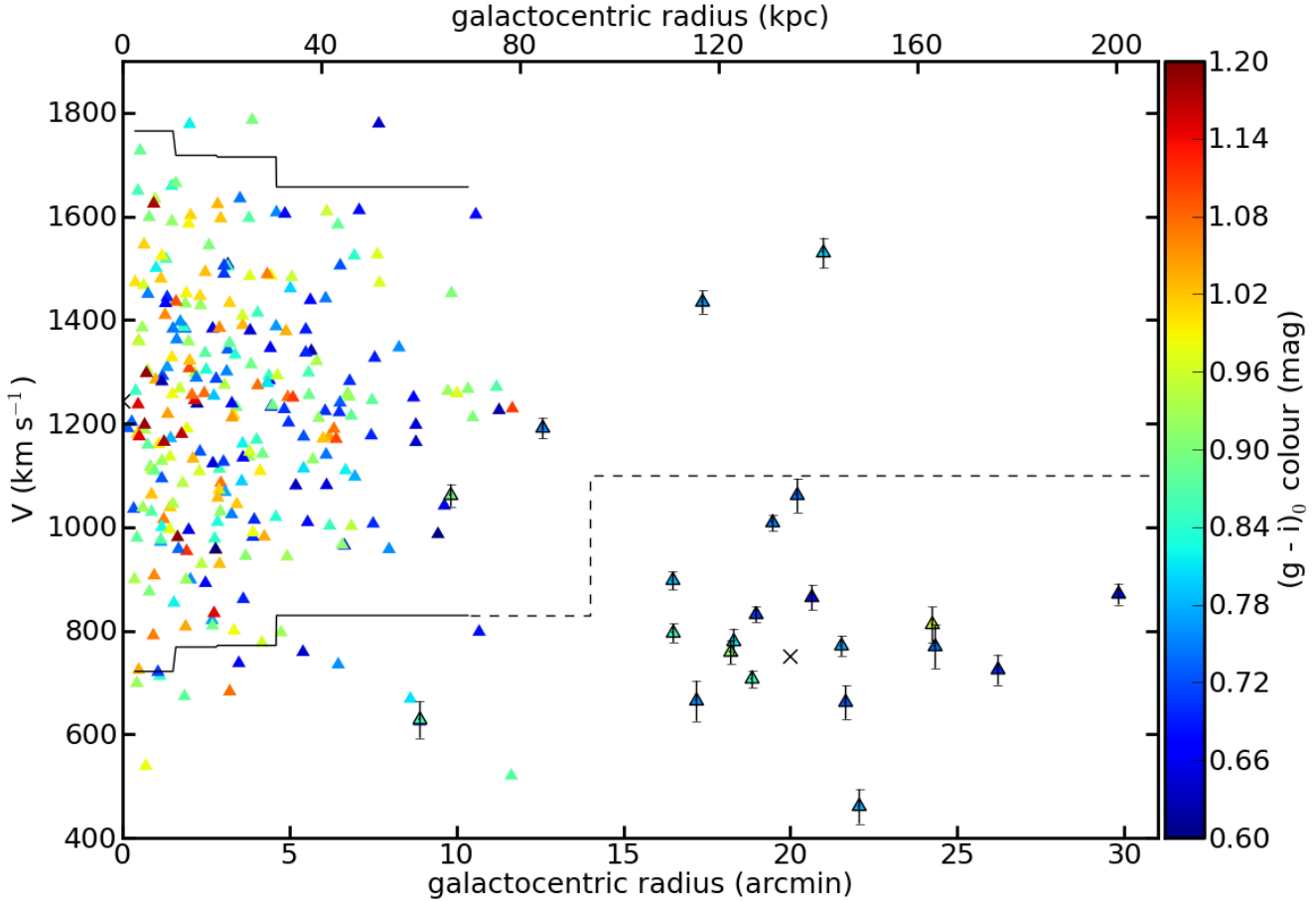


Figure 10. Phase-space diagram of globular cluster line-of-sight velocity as a function of distance from NGC 4365. New GC velocities presented here are shown as triangles with black outlines and error bars while previously published GC velocities (Blom et al. 2012b) are shown without. The colour of each symbol indicates its $(g - i)_0$ colour. NGC 4365 and NGC 4342 are marked with crosses at 0 arcmin, $V = 1243 \text{ km s}^{-1}$ and ~ 20 arcmin, $V = 751 \text{ km s}^{-1}$ respectively. The solid line shows the 2σ envelopes of the NGC 4365 GC velocity distribution and the dashed line indicates the adopted boundary, below which we classify objects as low velocity stream GCs. The 31 stream and NGC 4342 GCs have a similar mean velocity to NGC 4342. The $(g - i)_0$ colours of low velocity GCs are mostly blue with some green GCs but no red GCs. Red GCs are only found in the central regions of NGC 4365. The stream GCs are likely tidally stripped from the original GC system of NGC 4342.

3.3 GC system kinematics

The GCs that lie on the stream have a mean recession velocity of $682 \pm 22 \text{ km s}^{-1}$ and a velocity dispersion of $83 \pm 16 \text{ km s}^{-1}$. In Figure 11 these 14 stream GCs as well as 17 GCs more closely associated with NGC 4342 are plotted on an image of the stellar stream. The recession velocities of the GCs and nearby galaxies are marked by the colour of the points (i.e. NGC 4341: $V = 922 \text{ km s}^{-1}$, NGC 4343: $V = 1014 \text{ km s}^{-1}$, IC 3267: $V = 1231 \text{ km s}^{-1}$, IC 3259: $V = 1406 \text{ km s}^{-1}$). We note that NGC 4342 is the only galaxy in the area that has a low enough recession velocity to be consistent with the recession velocities of the GCs around it and extending along the stream. We see some indication of a possible velocity gradient along the stream but it is not possible to disentangle velocity shear along the GC stream from the effect of one-sided selection in velocity space, because NGC 4365’s GC system overlaps the GCs along the stream. Overall, the GC kinematics are consistent with a cold stream associated with NGC 4342.

The GCs close, and most likely bound, to NGC 4342

have a mean recession velocity of $790 \pm 40 \text{ km s}^{-1}$ and velocity dispersion of $139 \pm 37 \text{ km s}^{-1}$. If three GCs with 2σ velocities are excluded from the sample, the calculated velocity dispersion decreases to $\sim 75 \pm 23 \text{ km s}^{-1}$.

4 EFFECTS OF TIDAL STRIPPING

In this section we compare NGC 4342 to the locations of NGC 4486B and M32 on supermassive black hole (SMBH) and galaxy scaling relations. NGC 4486B and M32 are both well-known to be tidally stripped (Faber 1973; Graham 2002; Choi et al. 2002). In the case of M32 a giant stream of stars was detected by Ibata et al. (2001) which connects it (in projection) with M31 and another satellite galaxy, NGC 205. Deep imaging of the Virgo cluster core by Mihos et al. (2005) reveals that NGC 4486B lies in a region of substantial intracluster light and stellar streams, although no individual stream of stars can be easily assigned to NGC 4486B.

All three galaxies are known to deviate from the SMBH vs. spheroid mass relation and are relatively compact galax-

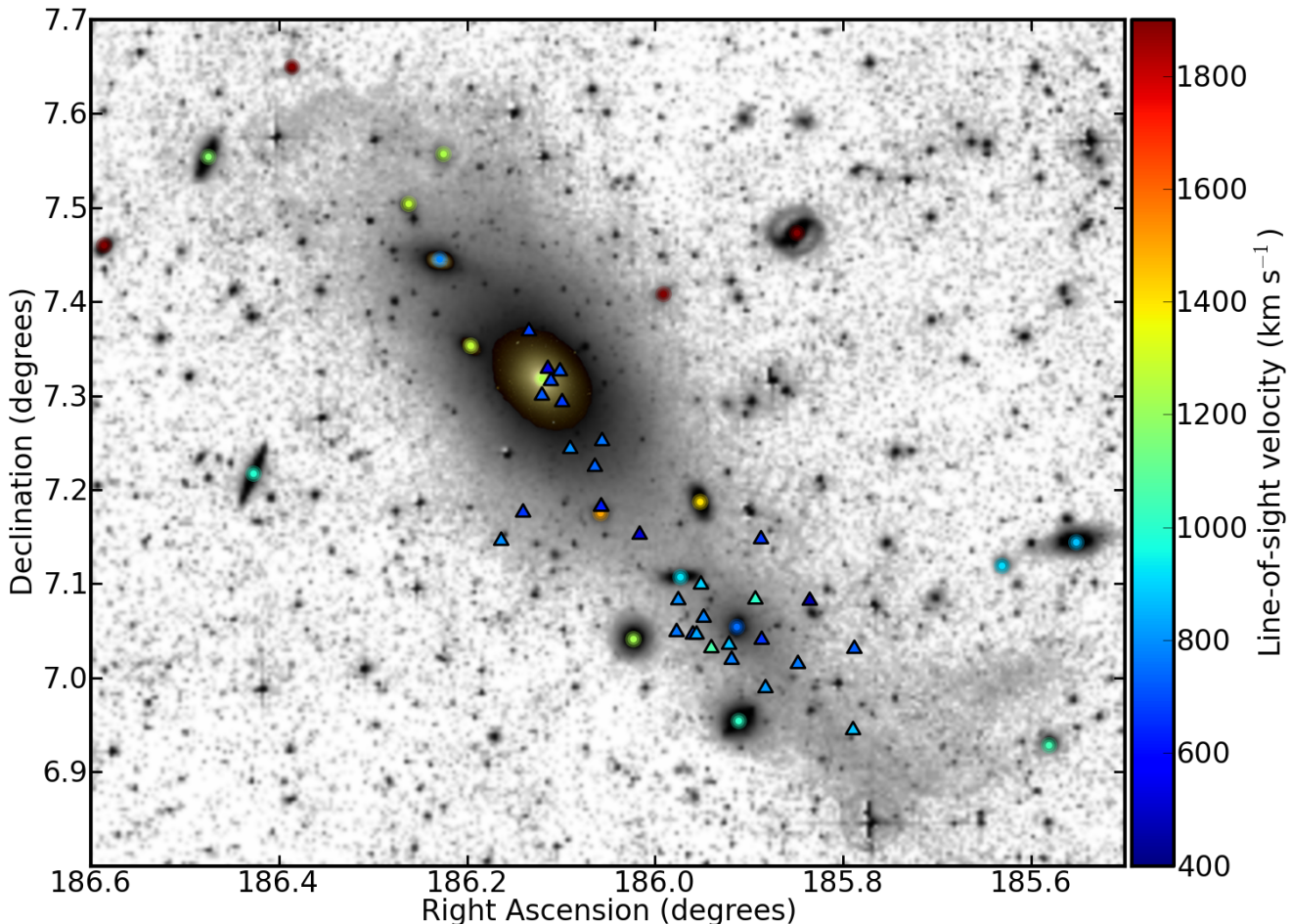


Figure 11. Deep optical imaging of the giant elliptical NGC 4365 and other nearby galaxies in the W' group, which reveals a ~ 300 kpc long stream of stars (Bogdán et al. 2012a). Globular clusters (GCs) in the stream are represented by triangles and galaxies by circles, with the colour of the points denoting their recession velocity (velocities > 1900 km s $^{-1}$ are assigned the reddest colour). The GCs have a mean velocity consistent with the recession velocity of NGC 4342 (located at R.A. $\sim 185.9^\circ$ and Dec. $\sim 7.05^\circ$) indicating that they were tidally stripped along with some stars from NGC 4342. The other galaxies in the W' group have recession velocities intermediate between those of NGC 4342 and NGC 4365 (i.e. NGC 4341: $V = 922$ km s $^{-1}$, NGC 4343: $V = 1014$ km s $^{-1}$, IC 3267: $V = 1231$ km s $^{-1}$, IC 3259: $V = 1406$ km s $^{-1}$).

ies with high central velocity dispersions. Their key properties are summarised in Table 2. Here we calculate spheroid (bulge) masses from their total K band magnitudes assuming that $M/L_K = 0.81$ (Bogdán et al. 2012a). SMBH masses are scaled by distance, from the original source, assuming a linear dependence. NGC 4486B is located in the Virgo cluster at a distance of 16.5 Mpc (Blakeslee et al. 2009). Its projected separation from central giant elliptical NGC 4486 (M87) is ~ 35 kpc. According to Gültekin et al. (2009) the SMBH mass determined by Kormendy et al. (1997) is somewhat uncertain. M32 is a close satellite of M31, for which we use a distance of 820 kpc. We note that M32 is the prototype of the compact elliptical (cE) class, which until recently included only half a dozen objects (Chilingarian et al. 2007).

The left panel of Figure 12 shows the SMBH mass vs. spheroid mass. For a galaxy undergoing tidal stripping of its outer stars, the luminosity will decrease, while the central properties will remain largely unchanged (Bender et al. 1992; Choi et al. 2002). In particular, we expect its SMBH mass and inner density profile to be unchanged, while its

total stellar mass is reduced. Although NGC 4342 is currently consistent with a single Sérsic profile (which is unlikely to have been modified by tidal stripping) we also include the core-Sérsic scaling relation from Scott, Graham & Schombert (2013). We show two extreme data points for NGC 4342, i.e. the small ($R_e = 96$ pc) bulge and the maximal bulge (the whole galaxy). NGC 4324, along with M32 and NGC 4486B, lies to the left of the standard Sérsic relation to a lower spheroid mass for a given SMBH mass. (We note that M32 has a bulge that is consistent with a Sérsic profile; Graham 2002.) In other words these galaxies all have a much higher SMBH mass as a fraction of their spheroid mass than the typical fraction of a percent for early-type galaxies (e.g. Gültekin et al. 2009; Graham 2012b). The effects of 50 percent and 75 percent stellar mass loss due to tidal stripping are shown.

Figure 12 also shows two other tight SMBH scaling relations – the stellar velocity dispersion near the centre of the galaxy (Graham 2012b) and the total number of globular clusters associated with a galaxy (Harris & Harris 2011).

Property	Value	Reference
NGC 4342	S0	1
Distance	23.1 Mpc	2
σ_0	241±10 km/s	3
R_e	672 pc	4a
R_e (bulge)	96 pc	4b
B_T^0	13.37 mag	1
M_B	-18.45 mag	-
K	8.9 mag	4a
K (bulge)	10.3	4b
Stellar mass	$2.5 \times 10^{10} M_\odot$	2
Stellar mass (bulge)	$6.9 \times 10^9 M_\odot$	2
[Fe/H]	0.25 dex	6
Black hole mass	$4.6^{+2.5}_{-1.5} \times 10^8 M_\odot$	7
Globular clusters	1200 ± 500	8
NGC 4486B	cE0	1
Distance	16.5 Mpc	9
σ_0	291±25 km/s	10
R_e	180 pc	11
B_T^0	14.26 mag	1
M_B	-16.83 mag	-
K	10.09 mag	5
Stellar mass	$4.3 \times 10^9 M_\odot$	2
[Fe/H]	0.13 dex	12
Black hole mass	$6.2^{+3}_{-2} \times 10^8 M_\odot$	10
M32	cE2	1
Distance	820 kpc	11
σ_0	76±10 km/s	11
R_e (bulge)	100 pc	11
B_T^0 (bulge)	9.23 mag	11
M_B (bulge)	-15.34 mag	-
Stellar mass (bulge)	$8.0 \times 10^8 M_\odot$	13
[Fe/H]	0.0 dex	14
Black hole mass	$2.9^{+0.6}_{-0.6} \times 10^6 M_\odot$	15

Table 2. Galaxy Properties. References are: (1) = de Vaucouleurs et al. (1991); (2) = this work, see text; (3) = Faber et al. (1989); (4a) = Vika (priv. comm.); (4b) = Vika et al. (2012); (5) = Skrutskie et al. (2006); (6) = van den Bosch et al. (1998); (7) = Cretton & van den Bosch (1999); (8) = Bogdán et al. (2012b); (9) = Blakeslee et al. (2009); (10) = Kormendy et al. (1997); (11) = Chilingarian et al. (2007); (12) = Sánchez-Blázquez et al. (2006); (13) = Häring & Rix (2004); (14) = Rose et al. (2005); (15) = Verolme et al. (2002).

For galaxies undergoing tidal stripping, the central velocity dispersion (σ_0) should be largely unchanged (Bender et al. 1992). Globular clusters (GCs) are fairly robust to galaxy interactions and mergers (their old ages indicating that many have survived a Hubble time, e.g. Strader et al. 2005). So although they will be stripped from the host galaxy (e.g. Bekki et al. 2003), a large area census should recover the original system population. Thus the *total* number of original GCs (N_{GC}) will also be unaffected by tidal stripping if a full census can be made. We expect the galaxies to be consistent with these scaling relations even if they have undergone tidal stripping. All three galaxies are fully consistent with the SMBH vs. velocity dispersion relation. In the case of NGC 4342, which has an estimate of its total original GC system (Bogdán et al. 2012b), it is also perfectly consistent with the GC scaling relation. Although the GC systems of the other galaxies have been studied, there is no estimate

available for the *total* number of GCs in the original GC system.

Further support for the tidal stripping hypothesis can be gained by comparing the galaxy stellar properties with those of normal galaxies and galaxies classified as compact ellipticals (which are generally thought to be the result of tidal stripping; Chilingarian et al. 2007). Figure 13 shows three key galaxy scaling relations as a function of B band galaxy luminosity, i.e. central velocity dispersion, central metallicity and effective radius. This figure shows that the three galaxies deviate from the standard scaling relations.

The figure also shows vectors representing the expected effects of 50 percent and 75 percent tidal stripping, assuming that size is reduced by the same proportions as per Bender et al. (1992) and that the central values of velocity dispersion and metallicity are unaffected. For the three subplots, each galaxy is consistent with having had their luminosity, stellar mass and size reduced by ~50-75 percent due to the effects of tidal stripping. Applying the stripping vectors to the current locations of the galaxies in Figure 13 suggests that the original progenitor galaxies were drawn from a large range in luminosity. It would clearly be of interest to obtain SMBH masses for a large sample of compact galaxies (see van den Bosch et al. 2012) to determine whether they lie systematically offset from the SMBH vs. spheroid mass relation in the sense as the three galaxies presented here.

The tidal stream around NGC 4365 detected by Bogdán et al. (2012a) shows an extensive (300 kpc) stellar stream with NGC 4342 lying near the centre of its SW arm. The stream has an integrated luminosity that is similar to NGC 4342 (Bogdán et al. 2012a). Since some stream light will be below the detection threshold, the stream mass is probably more than 50 percent of the current inferred mass of NGC 4342. If the stream has been tidally-stripped from NGC 4342 then the stellar mass loss is comparable to the amounts suggested by Figures 12 and 13.

Bogdán et al. (2012a) argued against tidal stripping of NGC 4342 for two reasons. The first is that a spheroid mass based on the K band surface brightness fits of Vika et al. (2012) indicated that over 90 percent of the galaxy stars would have to have been removed to explain its location in the SMBH vs. spheroid mass relation. Vika et al. (2012) fitted bulge and disk components. Their resulting bulge effective radius R_e was 0.86 arcsec, with a bulge mass of $6.7 \times 10^9 M_\odot$. However, the bulge size quoted by Vika et al. (2012) was only barely resolved given their seeing and sampling, and seems more akin to a nucleus given its physical size of 96 pc. A single component Sersic fit by Vika (priv. comm.) also gives a good fit to the K band data with $R_e = 6$ arcsec (similar to that measured by Faber et al. 1989, which we adopt here). The *total* K band magnitude gives a stellar mass of $2.5 \times 10^{10} M_\odot$ (similar to the value used by McConnell & Ma 2013 in their recent large sample SMBH analysis). Thus we have two extreme values for the spheroid mass of NGC 4342, i.e. using the same small bulge as Bogdán et al. (2012a) or the total galaxy as used by McConnell & Ma 2013 (with new photometry from Läsker et al. 2013 lying in between). These extremes are shown in Figure 12 and both values deviate strongly from standard SMBH vs. spheroid mass relations. NGC 4342 is consistent with 50-75 percent mass loss if the spheroid mass lies between the two extreme values given. A similar mass loss is suggested by the scaling

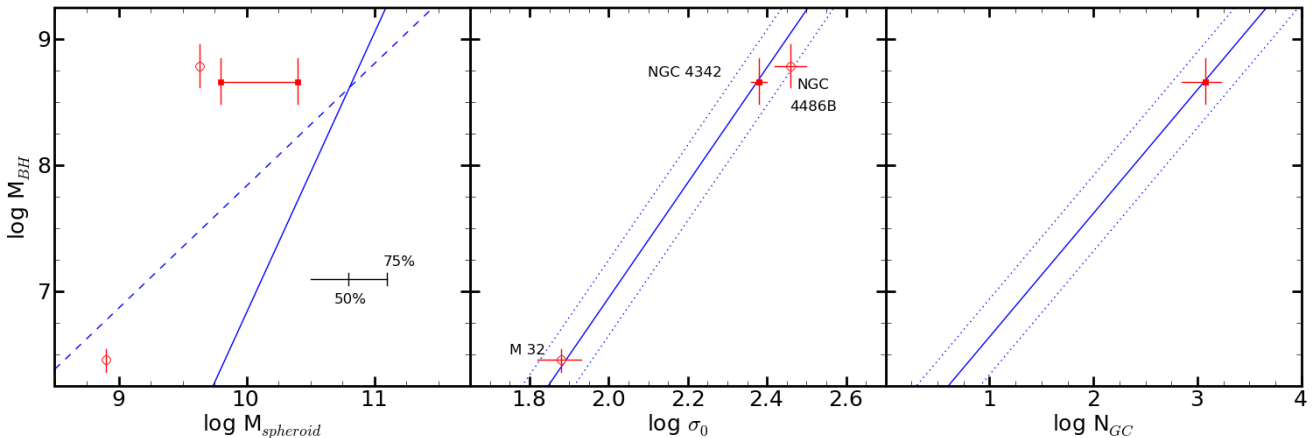


Figure 12. Supermassive black hole (SMBH) scaling relations. SMBH scaling relations (solid lines) from the literature are shown: **(Left)** spheroid mass in solar masses for core-Sersic (dashed) and Sersic (solid) profiles from Scott et al. (2013); **(Centre)** central velocity dispersion in km s^{-1} from Graham (2012b) for non-barred Sérsic galaxies; **(Right)** total number of globular clusters (GC) from Harris & Harris (2011). A representative intrinsic scatter of ± 0.3 dex for the velocity dispersion and GC scaling relations are shown by the dotted lines. NGC 4342 is shown by filled squares, with two spheroid masses representing the range in bulge mass. M32 and NGC 4486B are shown by open circles. The sample galaxies are labelled in the middle panel (with B for NGC 4486B). In the left panel the horizontal bar with vertical ticks shows the effect of 50 percent and 75 percent stellar mass loss from the original galaxy. All three galaxies are consistent with the central velocity dispersion scaling relation (and total number of globular clusters in the case of NGC 4342), whereas the galaxies deviate from the spheroid mass relation in the direction of substantial stellar mass loss due to tidal stripping.

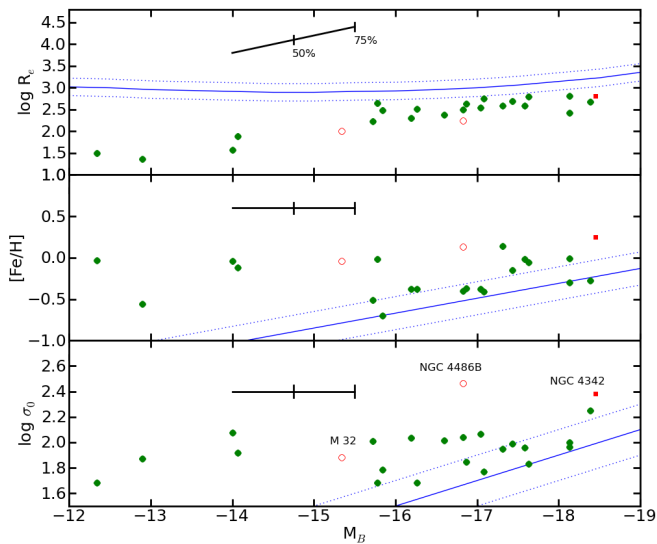


Figure 13. Galaxy scaling relations. Early-type galaxy scaling relations with B band luminosity (solid lines) from the literature are shown: **(Top)** effective radius in parsecs from Graham (2012a); **(Middle)** central metallicity from Chilingarian et al. (2008); **(Bottom)** central velocity dispersion in km s^{-1} from Matković & Guzmán (2005). A representative scatter of ± 0.2 dex for each scaling relation is shown by the dotted lines. Sample galaxies are shown by filled red circles and labelled in the lower panel. The location of compact elliptical galaxies (thought to be tidally-stripped) from the literature are shown by green filled circles. The bars with vertical ticks shows the effect of 50 percent and 75 percent stellar mass loss and size reduction due to tidal stripping. Tidal stripping will reduce the luminosity and the effective radius but the central velocity dispersion and central metallicity will remain largely unchanged. The galaxies are consistent with substantial stellar mass loss from the distribution of normal early-type galaxies.

relations shown in 13, and this is comparable to the estimated stellar mass in the stream. Although NGC 4342 may not have been stripped of 90 per cent of its mass, such high rates of mass loss may be appropriate for NGC 4486B and M32.

The second reason that Bogdán et al. (2012a) argued against tidal stripping is that dark matter in galaxy haloes has a lower binding energy on average than the stars and would generally be stripped first. Without a dark matter halo the galaxy would have difficulty retaining the hot X-ray emitting gas as observed (a point that will be examined further in the next Section). On the other hand, simulations suggest that stars can be stripped without the removal of *all* dark matter. From hydrodynamical simulations of small disk galaxies with Λ CDM-like haloes being stripped within a Virgo cluster-like potential, Goerdt et al. (2008) concluded that “*Even when the entire [baryonic] disk is tidally stripped away, the nucleus stays intact and can remain dark matter dominated even after severe stripping.*” In another case, Libeskind et al. (2011) simulated the mass stripped from small galaxies (subhaloes) located within the larger dark matter halo of a massive galaxy. They found that after a billion years, tidal stripping had indeed removed most of the dark matter, but 30 percent remained along with 60 percent of the original stellar mass (i.e. 40 percent of the stellar mass was stripped away). This work suggests that while most of the original dark matter is lost when half of the stars have been stripped away, a significant fraction (10 percent) of the dark matter can remain and would be likely to reside in the very central parts of the galaxy.

Despite these intriguing counterexamples, it may strain credibility to suppose that the stars in NGC 4342 have been almost completely stripped beyond a radius of $\sim 2\text{--}3$ kpc, while retaining a substantial dark matter halo out to at least $\sim 5\text{--}10$ kpc with no sign of truncation. However, there is a precedent in the mechanism of resonant stripping, which is

predicted to remove stars from the centres of dwarf galaxies while leaving their dark haloes intact (D’Onghia et al. 2009). In the D’Onghia et al. (2009) simulation of a small galaxy interacting with its hundred times larger neighbour, ~ 80 per cent of the stars were removed with little loss of dark matter. The simulations indicate that most of the stars would be removed from the galaxy’s disk, therefore it is likely, in this scenario, that NGC 4342 had a very extended disk that is now almost completely disrupted by tidal stripping. This also appears to be the case for M32 which reveals an ‘outer disk’ at large radii (Graham 2002; Choi et al. 2002). For NGC 4342 orbiting NGC 4365, the condition for resonance would imply a pericentric distance of ~ 10 – 20 kpc. To investigate such a possibility further, and to more generally resolve the question of whether or not hot gas and dark matter could be retained after tidal stripping, a tailored simulation is needed. This hydrodynamical simulation would need to include, at least, hot gas, stars and GCs embedded within the dark matter subhalo around NGC 4342 which is interacting with NGC 4365 within the overall dark matter and hot gas halo of the W' group.

Observational searches for dark matter around other tidally stripped galaxies could also be useful. In the case of M32, Howley et al. (2013) recently concluded that a dark matter halo was required to bind a small number of observed high velocity stars (with the caveat that they may not be in equilibrium). Thus despite the evidence for tidal stripping of stars from M32 (Graham 2002; Choi et al. 2002) it may still contain some dark matter.

5 DISCUSSION

The properties of the GC system around NGC 4342 suggest that the galaxy is being tidally stripped. We find a distribution of GCs peaked at the position of NGC 4342. Detailed analysis of the GC spatial distribution reveals a GC stream overlapping with NGC 4365’s GC system (NE of NGC 4342) and extending a roughly equal distance SW of NGC 4342. The $(g-i)_0$ colour distribution of the GCs close to NGC 4342 is indistinguishable from that of GCs in the stream and significantly different from that of NGC 4365’s GC colour distribution. This suggests that the stream GCs have been drawn from the outskirts of NGC 4342’s GC system. In addition to the similarity of their spatial and colour properties, the recession velocities of stream and NGC 4342 GCs ($V = 742 \pm 23 \text{ km s}^{-1}$) match the recession velocity measured from NGC 4342 starlight ($V = 751 \text{ km s}^{-1}$) very well.

Bogdán et al. (2012a) reported the presence of a stellar stream extending from the NE corner of NGC 4365 across the galaxy, through NGC 4342 and further SW. This stellar stream aligns well with the GC stream. Given the spatial and kinematic evidence, as well as the fact that NGC 4342 is a much less luminous galaxy ($M_B = -18.45 \text{ mag}$) than NGC 4365 ($M_B = -21.3 \text{ mag}$) it appears that NGC 4365 is tidally stripping NGC 4342 as it moves through the W' group.

Bogdán et al. (2012b) found X-ray evidence of hot gas (and ram pressure stripping of the gas) surrounding NGC 4342. They inferred a massive dark matter halo under the assumption of hydrostatic equilibrium for the hot gas not

affected by ram pressure stripping. Thus despite obtaining a mass profile out to ~ 40 kpc, they relied on the information within only ~ 10 kpc, and considered the equilibrium assumption still questionable in the ~ 5 – 10 kpc region. Within the ~ 2 – 5 kpc region where the mass profile should be more reliable, the dark matter component is inferred to be dominant, although we note that in other galaxies, X-ray based mass estimates have been found to be too high by factors of ~ 2 – 3 , even when the X-ray gas appears relatively relaxed (Romanowsky et al. 2009; Strader et al. 2011; Napolitano et al. 2013).

If the inferred X-ray mass is accurate, and NGC 4342 has a massive dark matter halo that extends far beyond the central luminous component, then it becomes difficult to explain a tidal stripping scenario, as discussed in the previous Section.

If the stars have instead been stripped off NGC 4365 and are in the process of accreting onto NGC 4342 we expect GCs from the outskirts of NGC 4365 to be accreting onto NGC 4342 as well. Given the measured recession velocities of NGC 4365, NGC 4342 and the stream GCs, this interpretation of the stream GCs originally coming from NGC 4365 is highly unlikely.

Further support for the tidal stripping scenario comes from investigation of NGC 4342 in the context of galaxy scaling relations and comparison to well known tidally stripped galaxies. NGC 4342 shows an offset from the black hole mass v.s. spheroid mass as well as effective radius/metallicity/central velocity dispersion vs. B band luminosity scaling relations in the same direction but to a lesser degree than NGC 4486B and M32. The scaling relation analysis shows it to be consistent with 50–75 percent stellar mass loss.

Finally, it is possible that the GCs and the stream came from a fully disrupted (now unseen) galaxy. If interaction with NGC 4342 has completely disrupted this galaxy and both its stars and GCs are now being accreted onto NGC 4342, there is no need for stars to be stripped from NGC 4342 before its dark matter halo. It is not far-fetched to assume a galaxy with an almost identical GC colour distribution to NGC 4342, since many galaxies have GC systems with similar colour distributions (Peng et al. 2006), but it might at first seem to be somewhat more problematic to also assume that such a galaxy had exactly the same recession velocity as NGC 4342. However, many of the galaxies around NGC 4342 have similar recession velocities and recent observations have shown that small galaxies accreting along streams or filaments might not be as uncommon as previously thought (Ibata et al. 2013). Nonetheless, the fully-disrupted galaxy scenario does not explain why the stellar properties of NGC 4342 match those of the stripped galaxies, M32 and NGC 4486B. The simplest interpretation is that the GCs and stars in the stream originated in NGC 4342.

6 CONCLUSIONS

We find an overdensity of globular clusters (GCs) centred on the S0 galaxy NGC 4342 that is spatially coincident with the stellar stream crossing NGC 4365, as reported by Bogdán et al. (2012a). The photometric colours of the stream GCs

match the colours of the GCs around NGC 4342 and their measured recession velocities ($V = 742 \pm 23 \text{ km s}^{-1}$) match the measured recession velocity of NGC 4342 itself ($V = 751 \text{ km s}^{-1}$). The evidence from these observations suggests that stars and GCs from NGC 4342 are being tidally stripped by the larger galaxy NGC 4365, situated at the centre of the W' group. When a wider array of stellar properties of NGC 4342 are considered, including black hole mass, metallicity and effective radius, it appears very similar to the well-known tidally stripped galaxies, NGC 4486B and M32. This finding is in tension with the conclusion that NGC 4342's stars and GCs have *not* have been stripped because it still hosts a large dark matter halo as inferred from observations of hot X-ray emitting gas (Bogdán et al. 2012b). Tailored simulations of NGC 4342, that include gas, stars and GCs within a dark matter halo are needed to reconcile all the evidence.

7 ACKNOWLEDGEMENTS

We thank the reviewer for helpful comments on the manuscript and thank P. Nulsen and B. Matthews for stimulating discussions. We also thank M. Smith, V. Pota, C. Usher, S. Kartha and N. Pastorello for support during the preparation of this manuscript. The data presented herein were obtained at the W.M. Keck Observatory, which is operated as a scientific partnership among the California Institute of Technology, the University of California and the National Aeronautics and Space Administration. The Observatory was made possible by the generous financial support of the W.M. Keck Foundation. The analysis pipeline used to reduce the DEIMOS data was developed at UC Berkeley with support from NSF grant AST-0071048. This research used the facilities of the Canadian Astronomy Data Centre operated by the National Research Council of Canada with the support of the Canadian Space Agency. CF acknowledges co-funding under the Marie Curie Actions of the European Commission (FP7-COFUND). This work was supported in part by NSF grants AST-0909237 and AST-1211995 as well as ARC Discovery grant DP130100388. DAF was supported by ARC grant DP130100388.

REFERENCES

- Bekki K., Forbes D. A., Beasley M. A., Couch W. J., 2003, *MNRAS*, 344, 1334
- Bender R., Burstein D., Faber S. M., 1992, *ApJ*, 399, 462
- Blakeslee J. P., Jordán A., Mei S., Côté P., Ferrarese L., Infante L., Peng E. W., Tonry J. L., West M. J., 2009, *ApJ*, 694, 556
- Blom C., Forbes D. A., Brodie J. P., Foster C., Romanowsky A. J., Spitler L. R., Strader J., 2012b, *MNRAS*, 426, 1959
- Blom C., Spitler L. R., Forbes D. A., 2012a, *MNRAS*, 420, 37
- Bogdán Á., Forman W. R., Kraft R. P., Jones C., Blom C., Randall S. W., Zhang Z., Zhuravleva I., Churazov E., Li Z., Nulsen P. E. J., Vikhlinin A., Schindler S., 2012b, *ApJ*, 755, 25
- Bogdán Á., Forman W. R., Zhuravleva I., Mihos J. C., Kraft R. P., Harding P., Guo Q., Li Z., Churazov E., Vikhlinin A., Nulsen P. E. J., Schindler S., Jones C., 2012a, *ApJ*, 753, 140
- Brodie J. P., Strader J., 2006, *ARA&A*, 44, 193
- Brodie J. P., Strader J., Denicoló G., Beasley M. A., Cenarro A. J., Larsen S. S., Kuntschner H., Forbes D. A., 2005, *AJ*, 129, 2643
- Chilingarian I., Cayatte V., Chemin L., Durret F., Laganá T. F., Adami C., Slezak E., 2007, *A&A*, 466, L21
- Chilingarian I. V., Cayatte V., Bergond G., 2008, *MNRAS*, 390, 906
- Choi P. I., Guhathakurta P., Johnston K. V., 2002, *AJ*, 124, 310
- Cooper M. C., Newman J. A., Davis M., Finkbeiner D. P., Gerke B. F., 2012, in *Astrophysics Source Code Library*, record ascl:1203.003 spec2d: DEEP2 DEIMOS Spectral Pipeline. p. 3003
- Côté P., Marzke R. O., West M. J., 1998, *ApJ*, 501, 554
- Cretton N., van den Bosch F. C., 1999, *ApJ*, 514, 704
- Daddi E., Renzini A., Pirzkal N., Cimatti A., Malhotra S., Stiavelli M., Xu C., Pasquali A., Rhoads J. E., Brusa M., di Serego Alighieri S., Ferguson H. C., Koekemoer A. M., Moustakas L. A., Panagia N., Windhorst R. A., 2005, *ApJ*, 626, 680
- Davies R. L., Kuntschner H., Emsellem E., Bacon R., Bureau M., Carollo C. M., Copin Y., Miller B. W., Monnet G., Peletier R. F., Verolme E. K., de Zeeuw P. T., 2001, *ApJ*, 548, L33
- de Vaucouleurs G., de Vaucouleurs A., Corwin Jr. H. G., Buta R. J., Paturel G., Fouqué P., 1991, *Third Reference Catalogue of Bright Galaxies. Volume I: Explanations and references. Volume II: Data for galaxies between 0^h and 12^h . Volume III: Data for galaxies between 12^h and 24^h .*
- D'Onghia E., Besla G., Cox T. J., Hernquist L., 2009, *Nature*, 460, 605
- Faber S. M., 1973, *ApJ*, 179, 423
- Faber S. M., Phillips A. C., Kibrick R. I., Alcott B., Allen S. L., Burrous J., Cantrall T., Clarke D., Coil A. L., Cowley D. J., Davis M., Deich W. T. S., Dietsch K., Gilmore D. K., Harper C. A., Hilyard D. F., Lewis J. P., McVeigh M., Newman J., Osborne J., Schiavon R., Stover R. J., Tucker D., Wallace V., Wei M., Wirth G., Wright C. A., 2003, in Iye M., Moorwood A. F. M., eds, *Society of Photo-Optical Instrumentation Engineers (SPIE) Conference Series Vol. 4841 of Society of Photo-Optical Instrumentation Engineers (SPIE) Conference Series*, The DEIMOS spectrograph for the Keck II Telescope: integration and testing. pp 1657–1669
- Faber S. M., Wegner G., Burstein D., Davies R. L., Dressler A., Lynden-Bell D., Terlevich R. J., 1989, *ApJS*, 69, 763
- Goerdt T., Moore B., Kazantzidis S., Kaufmann T., Macció A. V., Stadel J., 2008, *MNRAS*, 385, 2136
- Graham A. W., 2002, *ApJ*, 568, L13
- Graham A. W., 2012a, in , *Planets, Stars and Stellar Systems*. Springer
- Graham A. W., 2012b, *ApJ*, 746, 113
- Graham A. W., Driver S. P., 2005, *PASA*, 22, 118
- Grogin N. A., Geller M. J., Huchra J. P., 1998, *ApJS*, 119, 277
- Gültekin K., Richstone D. O., Gebhardt K., Lauer T. R., Tremaine S., Aller M. C., Bender R., Dressler A., Faber S. M., Filippenko A. V., Green R., Ho L. C., Kormendy J., Magorrian J., Pinkney J., Siopis C., 2009, *ApJ*, 698,

- 198
 Gwyn S. D. J., 2008, *PASP*, 120, 212
 Häring N., Rix H.-W., 2004, *ApJ*, 604, L89
 Harris G. L. H., Harris W. E., 2011, *MNRAS*, 410, 2347
 Howley K. M., Guhathakurta P., van der Marel R., Geha M., Kalirai J., Yniguez B., Kirby E., Cuillandre J.-C., Gilbert K., 2013, *ApJ*, 765, 65
 Ibata R., Irwin M., Lewis G., Ferguson A. M. N., Tanvir N., 2001, *Nature*, 412, 49
 Ibata R. A., Lewis G. F., Conn A. R., Irwin M. J., McConnachie A. W., Chapman S. C., Collins M. L., Fardal M., Ferguson A. M. N., Ibata N. G., Mackey A. D., Martin N. F., Navarro J., Rich R. M., Valls-Gabaud D., Widrow L. M., 2013, *Nature*, 493, 62
 Jiang F., van Dokkum P., Bezanson R., Franx M., 2012, *ApJ*, 749, L10
 Kormendy J., Bender R., Magorrian J., Tremaine S., Gebhardt K., Richstone D., Dressler A., Faber S. M., Grillmair C., Lauer T. R., 1997, *ApJ*, 482, L139
 Krajinovic D., Emsellem E., Cappellari M., Alatalo K., Blitz L., Bois M., Bournaud F., Bureau M., Davies R. L., Davis T. A., de Zeeuw P. T., Khochfar S., Kuntschner H., Lablanche P.-Y., McDermid R. M., Morganti R., Naab T., Oosterloo T., Sarzi M., Scott N., Serra P., Weijmans A.-M., Young L. M., 2011, *MNRAS*, 414, 2923
 Larsen S. S., Brodie J. P., Strader J., 2005, *A&A*, 443, 413
 Läscher R., Ferrarese L., van de Ven G., 2013, *ApJ*, in press, arXiv:1311.1530
 Libeskind N. I., Knebe A., Hoffman Y., Gottlöber S., Yepes G., 2011, *MNRAS*, 418, 336
 Matković A., Guzmán R., 2005, *MNRAS*, 362, 289
 McConnell N. J., Ma C.-P., 2013, *ApJ*, 764, 184
 Mihos J. C., Harding P., Feldmeier J., Morrison H., 2005, *ApJ*, 631, L41
 Napolitano N. R., Pota V., Romanowsky A. J., Forbes D. A., Brodie J. P., Foster C., 2013, *MNRAS*, submitted
 Newman J. A., Cooper M. C., Davis M., Faber S. M., Coil A. L., Guhathakurta P., Koo D. C., Phillips A. C., Conroy C., Dutton A. A., Finkbeiner D. P., Gerke B. F., Rosario D. J., Weiner B. J., Willmer C. N. A., Yan R., Harker J. J., Kassin S. A., Konidaris N. P., Lai K., Madgwick D. S., Noeske K. G., Wirth G. D., Connolly A. J., Kaiser N., Kirby E. N., Lemaux B. C., Lin L., Lotz J. M., Lupino G. A., Marinoni C., Matthews D. J., Metevier A., Schiavon R. P., 2012, *ArXiv e-prints*
 Peng E. W., Jordán A., Côté P., Blakeslee J. P., Ferrarese L., Mei S., West M. J., Merritt D., Milosavljević M., Tonry J. L., 2006, *ApJ*, 639, 95
 Pota V., Forbes D. A., Romanowsky A. J., Brodie J. P., Spitler L. R., Strader J., Foster C., Arnold J. A., Benson A., Blom C., Hargis J. R., Rhode K. L., Usher C., 2013, *MNRAS*, 428, 389
 Puzia T. H., Zepf S. E., Kissler-Patig M., Hilker M., Minniti D., Goudfrooij P., 2002, *A&A*, 391, 453
 Rhode K. L., Zepf S. E., 2004, *AJ*, 127, 302
 Romanowsky A. J., Strader J., Spitler L. R., Johnson R., Brodie J. P., Forbes D. A., Ponman T., 2009, *AJ*, 137, 4956
 Rose J. A., Arimoto N., Caldwell N., Schiavon R. P., Vazdekis A., Yamada Y., 2005, *AJ*, 129, 712
 Sánchez-Blázquez P., Gorgas J., Cardiel N., González J. J., 2006, *A&A*, 457, 809
 Schlegel D. J., Finkbeiner D. P., Davis M., 1998, *ApJ*, 500, 525
 Scott N., Graham A. W., Schombert J., 2013, *ApJ*, 768, 76
 Skrutskie M. F., Cutri R. M., Stiening R., Weinberg M. D., Schneider S., Carpenter J. M., Beichman C., Capps R., Chester T., Elias J., Huchra J., Liebert J., Lonsdale C., Monet D. G., Price S., Seitzer P., Jarrett T., Kirkpatrick J. D., Gizis J. E., Howard E., Evans T., Fowler J., Fullmer L., Hurt R., Light R., Kopan E. L., Marsh K. A., McCallon H. L., Tam R., Van Dyk S., Wheelock S., 2006, *AJ*, 131, 1163
 Smith R. J., Lucey J. R., Hudson M. J., Schlegel D. J., Davies R. L., 2000, *MNRAS*, 313, 469
 Spitler L. R., Forbes D. A., Strader J., Brodie J. P., Gallagher J. S., 2008, *MNRAS*, 385, 361
 Spitler L. R., Larsen S. S., Strader J., Brodie J. P., Forbes D. A., Beasley M. A., 2006, *AJ*, 132, 1593
 Strader J., Brodie J. P., Cenarro A. J., Beasley M. A., Forbes D. A., 2005, *AJ*, 130, 1315
 Strader J., Romanowsky A. J., Brodie J. P., Spitler L. R., Beasley M. A., Arnold J. A., Tamura N., Sharples R. M., Arimoto N., 2011, *ApJS*, 197, 33
 Surma P., Bender R., 1995, *A&A*, 298, 405
 Tonini C., 2013, *ApJ*, 762, 39
 van den Bosch F. C., Jaffe W., van der Marel R. P., 1998, *MNRAS*, 293, 343
 van den Bosch R. C. E., Gebhardt K., Gültekin K., van de Ven G., van der Wel A., Walsh J. L., 2012, *Nature*, 491, 729
 van Dokkum P. G., Franx M., Kriek M., Holden B., Illingworth G. D., Magee D., Bouwens R., Marchesini D., Quadri R., Rudnick G., Taylor E. N., Toft S., 2008, *ApJ*, 677, L5
 Verolme E. K., Cappellari M., Copin Y., van der Marel R. P., Bacon R., Bureau M., Davies R. L., Miller B. M., de Zeeuw P. T., 2002, *MNRAS*, 335, 517
 Vika M., Driver S. P., Cameron E., Kelvin L., Robotham A., 2012, *MNRAS*, 419, 2264
 West M. J., Côté P., Marzke R. O., Jordán A., 2004, *Nature*, 427, 31